RESEARCH PAPER

An Investigation into the Mechanical Properties of Aluminum Matrix Nanocomposite Reinforced with Graphene–Boron Nitride Hybrid

Behzad Rahimzadeh, Maisam Jalaly*, Mehrdad Roshan

* *maisam_jalaly@iust.ac.ir*

Nanotechnology Department, School of Advanced Technologies, Iran University of Science and Technology (IUST), Narmak, Tehran, 16846-13114, Iran

Received: September 2022 Revised: November 2022 Accepted: January 2023

DOI: 10.22068/ijmse.2982

Abstract: *Considering the widespread use of aluminum composites in various industries, aluminum-based nanocomposite samples reinforced with various percentages of graphene-BN hybrid powder were fabricated in this study. Initially, the graphene-BN hybrid was prepared and later subjected to wet milling together with aluminum powder. The final composite mixtures were consolidated using spark plasma sintering (SPS) method. Using this method, aluminum-based composite specimens containing 1 wt.% graphene–0 wt.% BN (AGB1), 0.95 wt.% graphene–0.05 wt.% BN (AGB2), 0.90 wt.% graphene–0.1 wt.% BN (AGB3), and 0.85 wt.% graphene–0.15 wt.% BN (AGB4) were prepared and compared with regard to their difference in mechanical properties. Hardness values of 48.1, 51.1, 56.2, 54.1, and 43.6 Hv were obtained for AGB0, AGB1, AGB2, AGB3, and AGB4, respectively. Additionally, tensile strengths of these specimens were 67.2, 102.1, 129.5, 123.7, and 114.7 MPa, respectively. Based upon the hardness and tensile test data, it was concluded that the AGB2 specimen had the highest tensile strength (93% higher than AGB0 and 27% higher than AGB1) and also higher hardness values (17% higher than AGB0 and 10% higher than AGB1).*

Keywords: *Nanocomposite, Aluminum, Graphene, Boron nitride*

1. INTRODUCTION

Metal matrix composites (MMCs) are composed of two components of a metal matrix (or an alloy of several metals) and a second phase, which is the reinforcing agent of the matrix. Metal-based composites have significant advantages over conventional materials, e.g. high mechanical strength and hardness, good resistance against corrosion, friction and wear, and high electrical and thermal conductivity [1]. Metal matrix nanocomposites are also referred to as materials either the metal/alloy matrix is nanostructured/nanocrystalline or a microcrystalline matrix reinforced by nanoparticles. MMCs reinforced by ceramic nanoparticles take advantages of high malleability and toughness of metals along with high Young's modulus and strength of the ceramic reinforcements. Therefore, metal matrix nanocomposites are appropriate candidates to fabricate industrial parts with high shear and compressive strengths [2].

Most of light metals like aluminum, magnesium, and titanium are commonly used as matrices in nanocomposites. Meanwhile, aluminum and its alloys are of great interest owing to their lower density, high electrical and thermal conductivity, and good corrosion resistance [3]. Regarding the relatively poor mechanical properties of aluminum compared to the other metals such as titanium, iron, and nickel, Al is often employed as an alloy or a composite [4, 5].

The matrix in the composite plays various roles, including connecting the reinforcements to each other and transferring the applied mechanical loads to the strong reinforcement. The ability to transfer compressive, bending, shear and tensile loads depends on the presence of the matrix as a load transfer medium, and the efficiency of this load transfer is directly influenced from the quality of the interfacial bond between the matrix and reinforcement. Moreover, the matrix must protect the second phase from mechanical damages and environmental and chemical attacks. In addition, a ductile matrix can also diminish or stop cracks originated from damaged reinforcements [2].

Various ceramic nanoparticles such as carbides, nitrides, oxides, and borides have been used to strengthen aluminum-based composites [6].

Carbon nanotubes and graphene have also been reported as the reinforcing agents for aluminum nanocomposites. Since graphene is highly reactive and prone to oxidative degradation at high temperatures, melting-based process is not a common route to produce aluminum matrix nanocomposites reinforced by graphene. To maintain the structural stability of graphene and prevent undesired reactions between graphene and aluminum, many fabrication processes are designed at temperatures which are sufficiently lower than Al melting point.

Alipour et al. [8] used a combination of ultrasonic treatment, powder metallurgy, and casting methods to produce aluminum alloy (7068) nanocomposite reinforced by graphene nanoplatelets (GNPs). In this method, aluminum powder was milled with GNP and the resultant was added to the molten Al. Later, the ultrasonic waves were used to achieve a uniform reinforcement dispersion inside the molten matrix. The addition of different amounts of GNP (0.1-1 wt. %) was studied in this research and concluded that increasing graphene up to 0.5 wt. % improved the mechanical properties, but further increase of the graphene content deteriorated the mechanical properties of the nanocomposite due to the agglomeration of GNPs. Wang et al. [9] also investigated the effect of graphene on the properties of aluminum-graphene nanocomposite. The ball-milled Al–0.5 wt. % graphene was consolidated in a graphite crucible with a pressure of 10 MPa and fired at 450°C followed by a second densification with a pressure of 40 MPa and sintered again at 600°C. As a result, the tensile strength and hardness were 30.6 and 44%, respectively, higher than those for the non-reinforced Al. Over the past few years, boron nitride (BN) has also been used as a reinforcement in the aluminum matrix nanocomposites. For example, Reddy et al. [10] prepared Al nanocomposite reinforced by BN nanoparticles (0.5, 1, and 1.5 vol. %) using the powder metallurgy method (2 hours of milling). The powder was compressed at a compaction pressure of ~510 MPa and sintered at 550°C using a microwave furnace to form cylindrical billets. Then their specimens were subjected to the hot extrusion process. A 36% increase in the tensile strength was observed for the specimen containing 1.5 wt. % BN.

Although graphene and boron nitride nanostructures were individually employed in the previous works to strengthen the Al matrix, the use of Gr-BN hybrid for strengthening aluminum has not been reported so far. Therefore, the novelty of the present study was the fabrication of a ternary nanocomposite consisted of aluminum reinforced by graphene-boron nitride hybrid and investigation of its mechanical properties.

2. EXPERIMENTAL PROCEDURE

In this research, Al powder from Merck Co. (Product No. GF01392050) with 99% purity and mean particle size of about 15 μm, commercial BN powder from Sigma-Aldrich Co. (Product No. 255475) with 98% purity and mean particle size of about 1 μm, few-layer graphene oxide (GO) suspension from Nanomavad Gostaran Pars Co. (NAMAGO, Iran) with a purity of 95%, hydrazine hydrate from Merck Co. with a purity of 50-60% (Product No. 225819), ethanol from Isfahan Zist Faravardeh Co. with a purity of 96%, and 24% ammonia solution from Dr. Mojallali Co. were provided as the initial materials. In general, the Al–Gr–BN nanocomposite was fabricated in three stages: (a) synthesis of graphene-boron nitride hybrid, (b) mixing the aluminum powder with the prepared hybrid through the mechanical milling method, (c) compression of the final nanocomposite powder and fabrication of the dense pellets using plasma spark sintering (SPS) method. All these steps will be described in detail below.

2.1. Preparation of Nanostructured Graphene-Boron Nitride Hybrid

In this stage, 200 mg of the commercial BN powder was subjected to the exfoliation using an ultrasonic horn in 200 ml ethanol for 2 h to obtain BN nanoparticles (nanolayers). After removing the alcohol, this product was washed and dried. Graphene-BN hybrids were made in three concentrations of 5, 10, and 15 wt. % BN. For instance, the RGO–5 wt. % BN specimen was prepared according to this protocol: 190 mg graphene oxide and 10 mg of ultrasonicated BN nanoparticles were mixed in 100 ml ethanol in the presence of 3 ml hydrazine hydrate and 3 ml ammonia solution. This mixture was stirred at 100°C for 2 h. In this procedure, the graphene oxide was reduced by hydrazine and ammonia at high temperature, and RGO nanosheets were deposited along with BN nanoparticles. The

resultant precipitate was collected, and after washing several times with distilled water, the final product was dried in an oven at 80°C. The other specimens with different BN concentrations were also prepared by the same method with corresponding amounts of initial GO and BN. Additionally, for the comparison purpose, the specimen RGO–0 wt. % BN (without BN) was fabricated following the same instruction.

2.2. Preparation of Al–RGO–BN Nanocomposite

In the final Al-based nanocomposite, the amount of the hybrid reinforcement (RGO–BN) was chosen to be fixed and equal to 1 wt. %. It is worth noting that the hybrid reinforcement had itself different BN content as described in section 2.1 (RGO–0, 5, 10, and 15 wt. % BN). To compare with composite specimens, the neat aluminum (without graphene and BN) was prepared according to the same procedure. The compositions of the all fabricated nano-composites are listed in Table 1. An appropriate amount of the prepared hybrid along with 5 g Al powder was ultrasonicated in the ethanol for 30 min. Then, ethanol-dispersed Al–RGO–BN mixture was wet-milled with steel balls for 2 h with the ball-to-powder ratio of 30:1 and rotation speed of 400 rpm. The milled powder was dried in an oven at 80°C.

Table 1. Specification of different nanocomposite specimens.

Specimen codes	Chemical composition (wt. %)		
	Al	RGO	BN
AGB0	100	0	0
AGB1	99	1	0
AGB2	99	0.95	0.05
AGB3	99	0.90	0.10
AGB4	99	0.85	0.15

2.3. Fabrication of Dense Pellets and Characterization

X-ray diffraction (XRD) analysis was used to distinguish graphene oxide (GO) and reduced graphene oxide (RGO) materials and to investigate the reduction process. This was performed by a Philips X'Pert PW1800 with a voltage of 40 kV and current of 30 mA using a Cu Kα with a wavelength of 1.5406 Å. The presence of the functional groups onto the GO and RGO were also analyzed using FTIR (SHIMADZU 8500S).

In order to determine the structural parameters of RGO and dried RGO–BN hybrid, Raman spectroscopy was performed using a dispersive Tachram Raman microscope (Iran) at a laser excitation wavelength of 532 nm (green laser). A field emission scanning electron microscope (FE-SEM, TESCAN-XMU MIRA3) was used to examine the surface morphology of the synthesized nanocomposite, the distribution of materials, and the fracture surface of the specimens. Furthermore, transmission electron microscope (TEM, EM 208S) was used to study the graphene-boron nitride hybrid.

The powder was converted to a dense pellet using the spark plasma sintering (SPS) method. An SPS60-10 apparatus (Iran) was used for the powder densification. The powder was sintered at 550°C for 10 min in a graphite die (30 mm in diameter) at the heating rate of 50°C/min and maximum pressure of 50 MPa under vacuum atmosphere.

The real densities of the consolidated specimens were measured using Archimedes' principle. The relative densities were calculated from dividing the real densities by the calculated densities. According to the ASTM E8/E8M, the sintered pellet was wire-cut to make the tensile specimen (Figure 1). To evaluate the mechanical properties, the sintered specimens were polished to obtain a smooth surface. The dumbbell-shaped specimens were loaded using a universal tensile equipment (SANTAM model 50-STM) at a strain rate of 0.2 mm/min. A Shab-Sari microhardness machine (model 5M) with an applied load of 25 g and a holding time of 15 s was used to measure the hardness of the densified nanocomposites.

3. RESULTS AND DISCUSSION

As mentioned in the Experimental section, graphene oxide (GO) suspension was initially used and converted to the reduced graphene oxide (RGO) using hydrazine and ammonia at 100°C to produce the RGO–BN hybrids. X-ray diffraction (XRD) analysis was employed to characterize and compare the GO before and after the reduction process.

Figure 2 (a) shows the XRD pattern for the GO. In general, the characteristic carbon peak in the pure graphite appears at $2\theta \approx 26°$, which corresponds to the (002) plane with an interlayer spacing of 0.34 nm [11, 12].

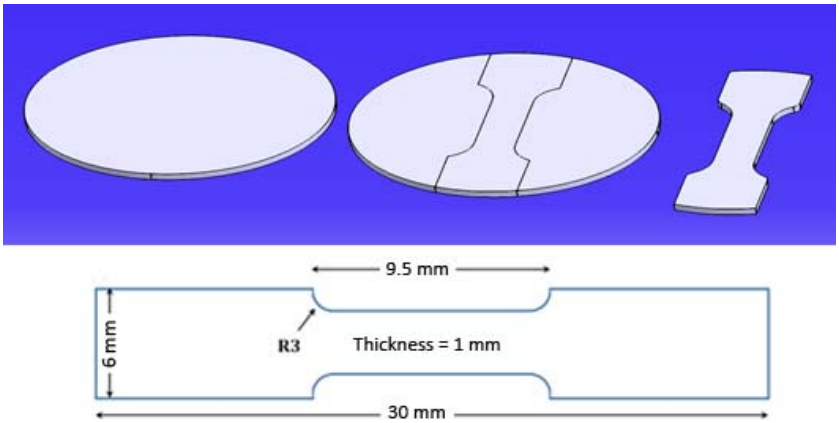

Fig. 1. Schematic of tensile specimen and its dimensions.

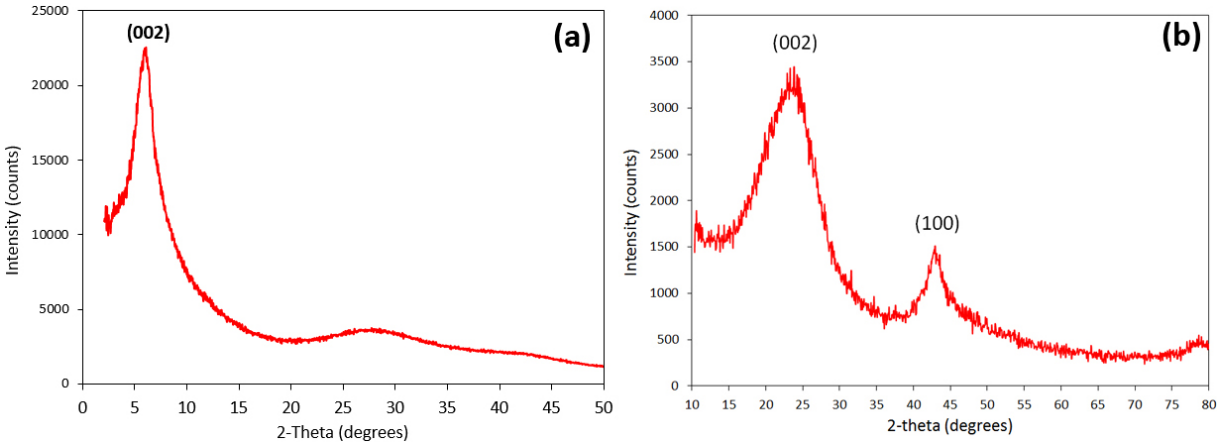

Fig. 2. XRD patterns of the (a) GO and (b) RGO

After chemical oxidation of the graphite, the 2θ peak shifts to the lower angles of ~ 7–10°, depending on the oxidation level, indicating the full oxidation of graphite into the GO with a d-spacing of ~ 0.86–0.93 nm. The increase in d-spacing results from the formation of oxygenated functional groups such as carbonyl, epoxy, hydroxyl, and carboxyl between the graphite layers due to the oxidation processing [11–13]. In the present study, hydrazine hydrate as the chemical reducing agent was added to the GO suspension. The main indicator for the conversion of the initial GO to the RGO in the XRD pattern is the peak shift to the lower angles. Fig. 2 shows the XRD patterns for the GO and RGO. As can be seen, the characteristic peak of the GO observed at 2θ ≈ 7° (Fig. 2 (a)) shifted to 2θ ≈ 25° (Fig. 2 (b)), which corresponds to the RGO [11]. Using Bragg's relation, the distance between the (002) planes in the RGO was calculated to be 0.38 nm, which is close to the interlayer spacing (d) in graphite. Also, the broad appearance of the (002) peak in the RGO pattern implies the irregular distribution of graphene layers and its damaged structure due to the chemical reduction. As shown in Fig. 2 (b), there is another peak with lower intensity at 2θ= 45°, which is a fingerprint peak for the (100) crystal plane of the graphite lattice. The appearance of this peak also confirms the re-generation of the graphitic nanocrystals on the graphene layers after the GO reduction.

FTIR spectra of GO and RGO are shown in Figure 3. The transmittance bands of the GO spectrum appeared at wavenumbers of about 1700, 1600, 1380, and 1058 cm^{-1} are related to the stretching vibrations of the C=C bond, O=C carbonyl group, C–OH group, and C–O bond in the epoxy group, respectively. In addition, the bands located at about 3100 and 3600 cm^{-1} are attributed to the stretching vibration of C–H and hydroxyl O–H bonds, respectively [14, 15]. Comparing the FTIR spectra of GO and RGO shows that the main oxygenated functional groups like O=C and O–H bonds were removed and the

band intensity ofC–O and C–OH groups decreased, while the band intensity of C=C bond increased.
This implies an appropriate reduction of GO and significant removal of surface moieties, although the reduction process is not complete which is frequently reported by others [14, 15].

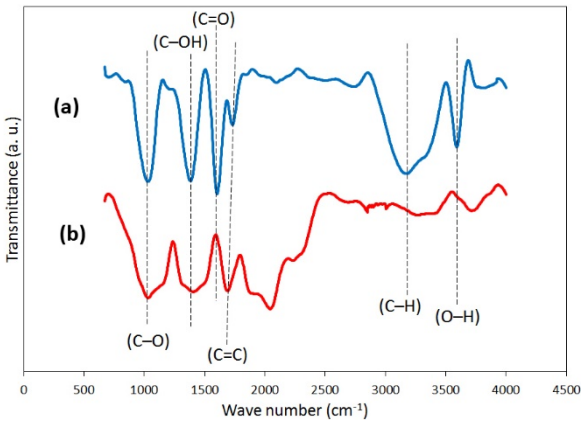

Fig. 3. FTIR spectra of the (a) GO and (b) RGO.

Figure 4 shows the XRD patterns of the commercial BN and RGO–BN hybrid. All peaks located at ~ 26.5°, 41°, 43°, 50°, 55°, and 76° (Figure 4 (a)) correspond to the crystallographic planes of (002), (100), (101), (102), (004), and (110), respectively, in the BN lattice ((ICDD PDF #34-0421). BN has a hexagonal crystal structure and the distance between (002) planes is 3.33 Å [16]. As shown in Figure 4 (b), the RGO–BN hybrid has an appropriate crystal structure. This figure contains both features seen in the patterns shown in Figure 2 (b) and 4 (a). In addition to the BN peaks, the broad peak at ~25° belongs to the RGO, indicating the formation of the hybrid structure between RGO and BN [17].

The representative Raman spectra of the RGO and RGO–BN hybrid are shown in Figure 5. Graphene exhibited two characteristic peaks at 1361 and 1598 cm^{-1} (Figure 5 (a)), which are related to the D and G bands in the Raman spectrum, respectively. The D peak in the Raman spectrum is an indicator of the lattice disorder originated from the structural defects like vacancies, grain boundaries, and oxygenated surface groups to the carbon basal plane [18].
The G band is the characteristic peak for the carbon network, which originates from the in-plane stretching bonds of the sp^2-hybridized carbon pairs. This peak indicates the degree of graphitic structure in the carbonaceous material. The intensity ratio of the D band to G band (ID/IG) indicates the oxidation degree in the carbon network and the defect density in the graphene structure [11, 18]. Based on Figure 5 (b), the RGO–BN hybrid also has two distinct peaks at 1368 and 1607 cm^{-1}, suggesting a negligible shift compared to those of the RGO Raman spectrum. This indicates that the graphene structure is robust and unchanged during the chemical processing, which is in accordance with that reported by Li et al. [17]. A slight Raman shift to the higher values in the hybrid specimen compared to the RGO suggests a small change in the electronic properties of graphene by adding boron nitride [17, 18]. The ID/IG parameter was 1 and 1.13 for the RGO and RGO–BN hybrid, respectively. It shows that the amount of disorder in the hybrid structure is higher than that of the RGO. It can be inferred that BN nanoparticles have entered into the accumulated graphene layers and located at their surfaces.

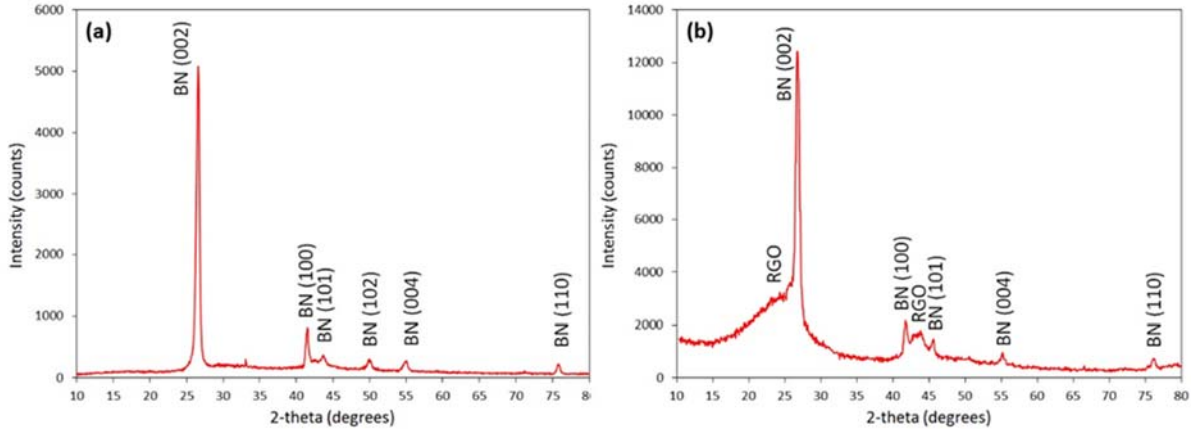

Fig. 4. XRD pattern of (a) commercial boron nitride, (b) RGO-BN hybrid.

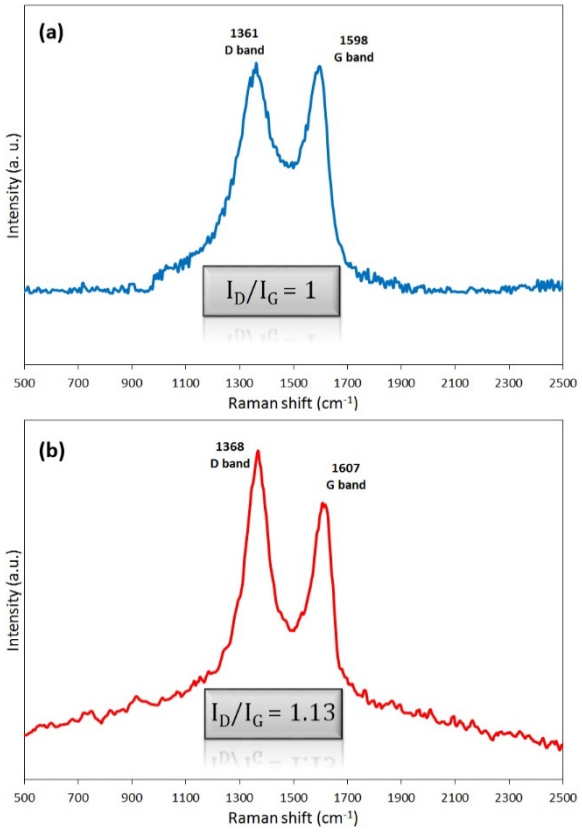

Fig. 5. Raman spectra for the (a) RGO and (b) RGO–BN hybrid.

This disrupts the structural order and well-arranged configuration of the graphene network, which changes the surface morphology and forms the surface wrinkles [17].

Figure 6(a) shows the transmission electron microscopy (TEM) image of BN nanoparticles after ultrasonication for 2 h. As seen, commercial micron-sized BN particles have been exfoliated due to the robust ultrasonic waves and converted into the nanoparticles with diameters of about 100–150 nm. The morphology of initial GO nanosheets is shown in Figure 6(b). Graphene nanosheets with a high transparency, wrinkled surface, and folded edges are clearly observed, which has frequently been reported as a normal nature of the graphene [19]. Furthermore, Figure 6(c) depicts the TEM image of the RGO–BN hybrid. BN nanoparticles are surrounded by the graphene nanosheets to form an encapsulation-like morphology. The formation of this structure is due to the application of ultrasonic waves to the combination of these two materials (graphene and BN), which causes the BN nanoparticles to be enwrapped by the flexible graphene nanosheets.

All Al-based powder nanocomposites were consolidated by the SPS technique, as described in the experimental section, and their mechanical properties were investigated.

The relative densities of the consolidated specimens were calculated to be in the range of 94-96%. Since the content of the reinforcing agents was so small, there was no considerable difference between density data for different specimens. As can be seen in Figure 7, the hardness of the AGB1 specimen, which has only graphene reinforcement, increased by about 6.2% compared to that of the neat aluminum specimen (AGB0). By adding 0.05 wt. % BN, the AGB2 specimen exhibited ~16.8% and ~10% increase in the hardness compared to that of the AGB0 and AGB1, respectively. This shows that adding BN nanoparticles has a significant positive effect on the hardness of the nanocomposite structure containing RGO. Based on Figure 7, the hardness of the Al-based nanocomposite decreased for AGB3 (0.1 wt. % BN) and AGB4 (0.15 wt. % BN) specimens. Therefore, higher reinforcement concentrations caused a destructive effect on the hardness feature. The decrease in the hardness in the AGB3 and AGB4 specimens with higher BN contents may be attributed to more agglomeration of the reinforcement and the creation of stress concentration sites in the composite. Figure 8(a) shows the stress-strain diagrams of all specimens obtained from the tensile test.

The curve for the neat aluminum (AGB0) represents a typical behavior for a ductile metal with a large plastic section (high fracture strain). However, the nanocomposite specimens exhibit a quasi-brittle behavior, in which the maximum strength increased due to the high mechanical properties of nanoscale additives, and their fracture strain decreased significantly. Figure 8(b) shows the changes in the tensile strength and elongation values of different specimens. It can be observed that the AGB1 specimen with 1 wt. % RGO as the reinforcement exhibited a 52% increase in the tensile strength compared to that of the neat aluminum (AGB0). Additionally, the tensile strength of AGB2 with 0.95 wt. % RGO and 0.05 wt.% BN was ~93 and 27% higher than that for AGB0 and AGB1 specimens, respectively. This suggests the influential role of adding BN nanoparticles to the nanocomposite structure containing RGO. AGB3 and AGB4 specimens (with 0.1 and 0.15 wt. % BN, respectively) exhibited a reduction in the tensile strength.

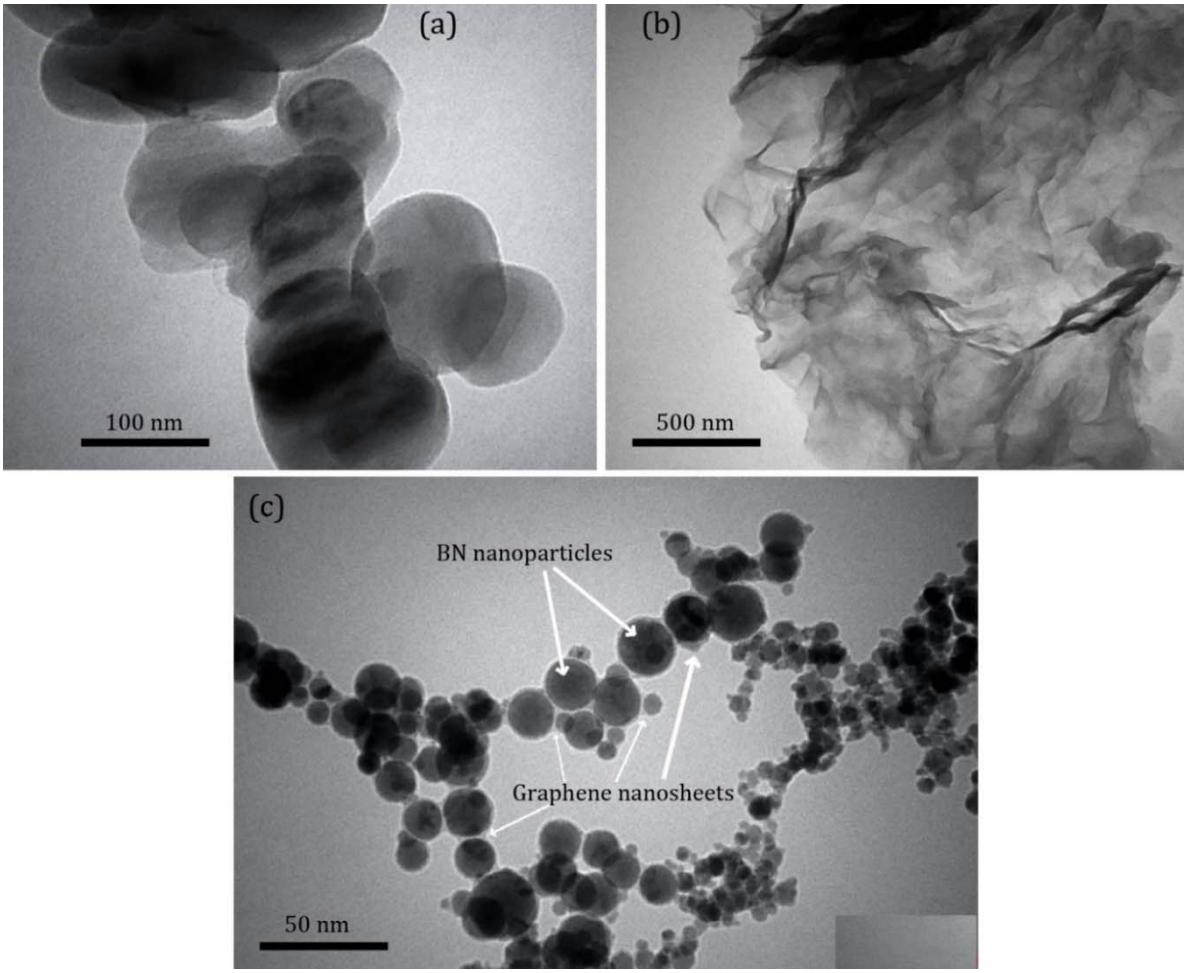

Fig. 6. TEM images of the (a) BN nanoparticles after ultrasonication for 2 h, (b) initial GO nanosheets, and (c) RGO–BN hybrid.

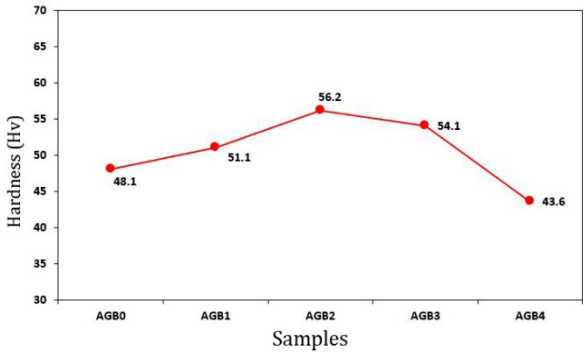

Fig. 7. Hardness of various composite specimens.

Regarding AGB3 and AGB4 specimens with higher amounts of BN, the decrease in the tensile strength may ascribed to the reinforcement aggregation and the formation of stress concentration sites in the composite.

Consequently, the AGB2 specimen showed the highest mechanical properties and was chosen as the best specimen in terms of mechanical behavior. In addition, the elongation of all nanocomposite specimens (AGB1, AGB2, AGB3, and AGB4) decreased considerably (about 70%) compared to the AGB0 indicating a shift in mechanical behavior from ductile to brittle by adding just 1 wt. % nanostructured reinforcement. As shown, nanostructured reinforcement has the substantial impact on the strengthening of aluminum. This is due to the role of these nanoscale structures in stopping or slowing down the movement of dislocations and reducing micro/nanopores created during the sintering process [20]. Furthermore, graphene can restrict Al grain growth in the sintering process by Zener pinning mechanism. Thus, adding graphene to the metallic matrix can form a refined structure, leading to enhanced mechanical properties (like AGB1 in comparison with AGB0).

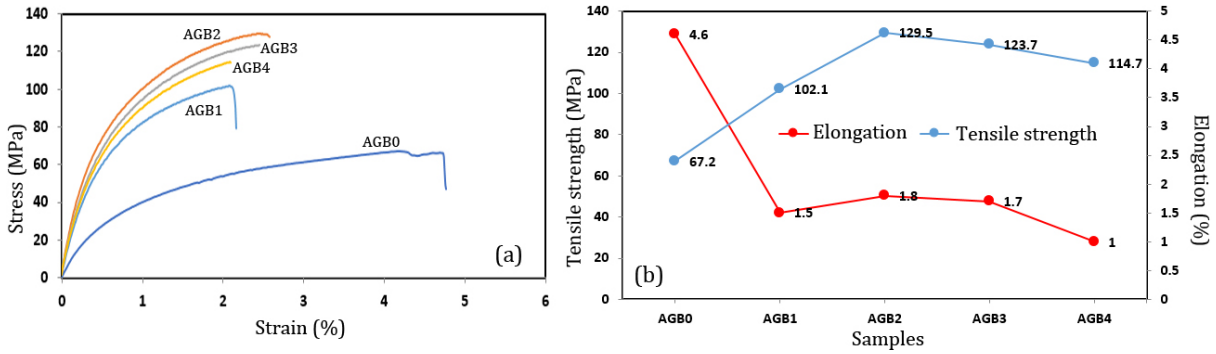

Fig. 8. (a) Stress-strain curves for different Al–RGO–BN nanocomposite specimens. (b) Variations of the tensile strength and elongation for different specimens.

Moreover, wrinkling and folding of graphene nanosheets can provide a good mechanical interlocking with Al matrix, resulting in a restriction in its plastic deformation [21].

The improvement of mechanical properties in case of the best specimen (AGB2) compared to the AGB1 specimen (containing only graphene as the reinforcement) may be attributable to the fact that BN nanoparticles are enclosed between the graphene nanosheets, which strengthens the barrier against the movement of dislocations and microcracks (the main factors for the failure). Therefore, dislocations/cracks for passing these obstacles (nanoscale reinforcement) require higher forces, meaning the higher strength. However, the tensile strength decreased with further increase of the BN content in the hybrid reinforcement (AGB3 and AGB4).

It seems that by increasing boron nitride concentration in the reinforcement, the uniform distribution of these nanoparticles was disrupted, forming larger aggregates of nanoparticles surrounded by graphene. These aggregates can be more prone to stress concentration and cause new microcracks against lower applied loads, reducing the overall strength.

The SEM micrographs from the fracture surfaces of AGB0, AGB1, and AGB2 are shown in Figure 9. Dimple fracture, as a clear measure for the ductile failure, is observed in the fracture surface of the neat aluminum. The nanocomposite specimens also showed similar fracture surfaces with a dimple structure, but dimples and grains were smaller due to the presence of nanostructured reinforcements, which improved the mechanical properties of the nanocomposite.

Figure 10(a) shows the fracture surface of the best specimen (AGB2). The elemental distribution maps for aluminum, carbon, nitrogen, and boron are also shown in this figure. As seen in Figure 10(c), the elemental analysis indicates the distribution of carbon throughout the matrix, and specifically, an interlocked mass of graphene nanosheets is clearly identifiable in the center of the image. Based on Figures 10 (d) and (e), nitrogen and boron can be recognized in the whole of the matrix. An accumulation of nitrogen and boron can be identified on the central graphene flakes, implying the appropriate performance of the used processes for the preparation of RGO–BN hybrid.

4. CONCLUSIONS

In this research, after preparation of RGO–BN hybrid, the nanocomposite powder of Al–RGO–BN was prepared by wet ball-milling method. Al matrix nanocomposite powder mixtures were consequently densified by the SPS technique.

According to the mechanical results, values of 102, 129, 123, and 114 MPa were achieved for the tensile strength of AGB1, AGB2, AGB3, and AGB4 specimens, respectively, which were 52, 93, 84, and 71% higher than that of the neat Al specimen sample (67.2 MPa), respectively. The specimen AGB2 exhibited the highest tensile strength and its elongation was about 1.8%. Additionally, AGB2 showed the highest hardness value of 56.2 Hv in the microhardness test Therefore, AGB2 nanocomposite specimen with the chemical composition of Al–0.95 wt. % RGO–0.05 wt.% BN was chosen to be the best sample in terms of mechanical properties. According to the electron microscopy micrographs, grain refinement and mutual effects of BN nanoparticles with graphene nanosheets inside the aluminum matrix were the possible

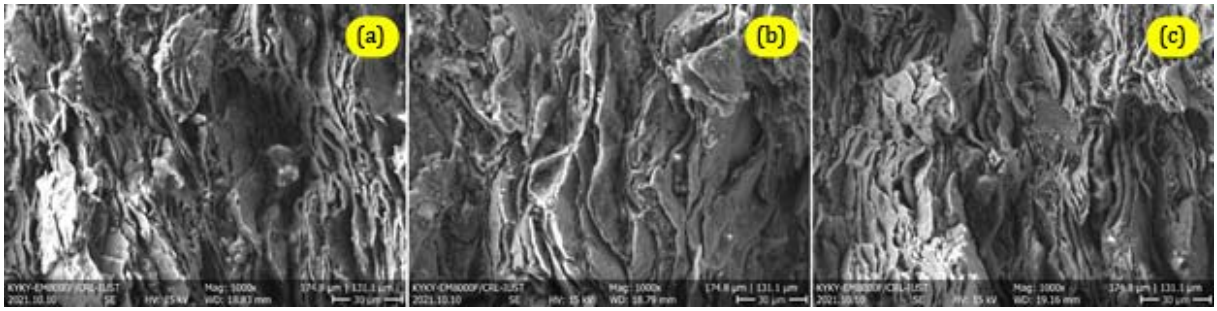

Fig. 9. SEM micrographs from the fracture surfaces of the different specimens: (a) AGB0, AGB1, and AGB2.

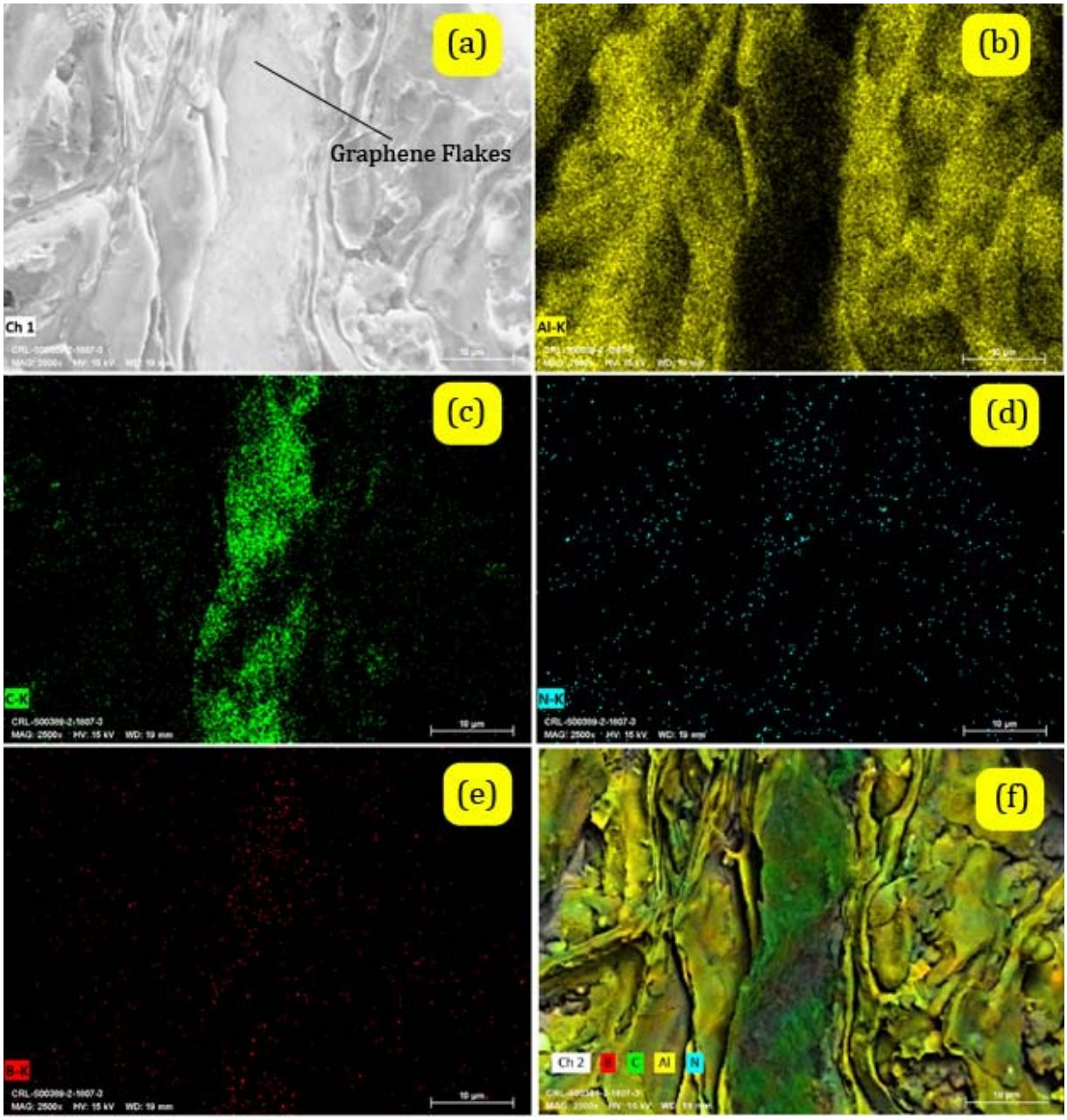

Fig. 10. (a) Representative SEM micrograph of the fracture surface of the densified AGB2 nanocomposite. Elemental mappings for (b) Al, (c) C, (d) N, (e) B and (f) overlay.

cause of the improved mechanical properties of the AGB2 specimen. However, mechanical properties of the densified nanocomposites decreased at higher BN concentrations (AGB3 and AGB4) which might be due to the agglomeration and non-uniform distribution of the reinforcement phase in the matrix.

REFERENCES

[1]. Rawal, S., "Metal-matrix composites for space applications", JOM, 2001, 53, 14-17.

[2]. Ajayan, P. M., Schadler, L. S. and Braun, P. V., "Nanocomposite: Science and Technology", Wiley, New York, 2003, p. 1-20.

[3]. Joel, J. and Xavior, M. A., "Aluminium alloy composites and its machinability studies; a review", Mater. Today: Proc., 2018, 5, 13556-13562.

[4]. Fuller, C. B., Mahoney, M. W., Calabrese, M. and Micona, L., "Evolution of microstructure and mechanical properties in naturally aged 7050 and 7075 Al friction stir welds", Mater. Sci. Eng.: A, 2010, 527, 2233-2240.

[5]. Yang, D., Feng, N., Wang, Y. and Wu, X., "Preparation of primary Al-Si alloy from bauxite tailings by carbothermal reduction process", Trans. Nonferrous Met. Soc. China, 2010, 20, 147-152.

[6]. Jafarpour, S. R. and Pakshir, M., "Evaluation of microstructure, mechanical properties and corrosion of Al matrix nanocomposite reinforced by SiC nanoparticles", Nanomaterials, 2012, 15, 187-195 (In Persian).

[7]. Liang, A., Jiang, X., Hong, X., Jiang, Y., Shao, Z. and Zhu D., "Recent developments concerning the dispersion methods and mechanisms of graphene", Coatings, 2018, 8, 33.

[8]. Alipour, M. and Eslami-Farsani, R., "Synthesis and characterization of graphene nanoplatelets reinforced AA7068 matrix nanocomposites produced by liquid metallurgy route", Mater. Sci. Eng.: A, 2017, 706, 71-82.

[9]. Wang, J., Guo, L., Lin, W., Chen, J., Liu, C., Chen, S., Zhang, S. and Zhen, T., "Effect of the graphene content on the microstructures and properties of graphene/aluminum composites", New Carbon Mater., 2019, 34, 275-285.

[10]. Reddy, M. P., Manakari, V., Parande, G., Ubaid, F., Shakoor, R. A., Mohamed, A. M. A. and Gupta, M., "Enhancing compressive, tensile, thermal and damping response of pure Al using BN nanoparticles", J. Alloys Compds., 2018, 762, 398-408.

[11]. Chen, W. and Yan, L., "In situ self-assembly of mild chemical reduction graphene for three dimensional architectures", Nanoscale, 2011, 3, 3132-3137.

[12]. Cui, P., Lee, J., Hwang, E. and Lee, H., "One-pot reduction of graphene oxide at subzero temperatures", Chem. Commun., 2011, 47, 12370-12372.

[13]. Thakur, S. and Karak, N., "Green reduction of graphene oxide by aqueous phytoextracts", Carbon, 2012, 50, 5331-5337.

[14]. Faniyi, I. O., Fasakin, O., Olofinjana, B., Adekunle, A. S., Oluwasusi, T. V., Eleruja, M. A. and Ajayi, E. O. B., "The comparative analyses of reduced graphene oxide (RGO) prepared via green, mild and chemical approaches", SN Appl. Sci., 2019, 1, 1181.

[15]. Lu, J., Li, Y., Li, S. and Jiang, S. P., "Self-assembled platinum nanoparticles on sulfonic acid-grafted graphene as effective electrocatalysts for methanol oxidation in direct methanol fuel cells", Sci. Rep., 2016, 6, 21530.

[16]. Matović, B., Luković, J., Nikolić, M., Babić, B., Stanković, N., Jokić, B. and Jelenković, B., "Synthesis and characterization of nanocrystaline hexagonal boron nitride powders: XRD and luminescence properties", Ceram. Int., 2016, 42, 16655-16658.

[17]. Li, Y., Li, Z., Zhai, J., Zhao, L., Chen, J. and Meng, F., "Synthesis, microstructure and thermal stability of graphene nanoplatelets coated by hexagonal boron nitride (h-BN)", Mater. Chem. Phys., 2019, 221, 477-482.

[18]. Tuz Johra, F., Lee, J. and Jung, W. G., "Facile and safe graphene preparation on solution based platform", J. Ind. Eng. Chem., 2014, 20, 2883-2887.

[19]. Fasolino, A., Los, J. H. and Katsnelson, M. I., "Intrinsic ripples in graphene", Nat. Mater., 2007, 6, 858-861.
[20]. Tian, W., Li, S., Wang, B., Chen, X., Liu, J. and Yu, M., "Graphene-reinforced aluminum matrix composites prepared by spark plasma sintering", Int. J. Miner. Metall. Mater., 2016, 23, 723-729.
[21]. Bisht, A., Srivastava, M., Kumar, R. M., Lahiri, I. and Lahiri, D., "Strengthening mechanism in graphene nanoplatelets reinforced aluminum composite fabricated through spark plasma sintering", Mater. Sci. Eng.: A, 2017, 695, 20-28.